PCCP

Accepted Manuscript

ROYAL SOCIETY OF CHEMISTRY

www.rsc.org/pccp

Journal Name

RSCPublishing

ARTICLE

A carbazole-fluorene molecular hybrid for quantitative detection of TNT with combined fluorescence and quartz crystal microbalance methods

Cite this: DOI: 10.1039/xoxxoooooox

Received ooth January 2012,
Accepted ooth January 2012

DOI: 10.1039/xoxxoooooox

www.rsc.org/

Kalathil K. Kartha,[a] Anjamkudy Sandeep,[a] Vijayakumar C. Nair,[a] Masayuki Takeuchi*[b] and Ayyappanpillai Ajayaghosh*[a]

A combined fluorescence and quartz-crystal microbalance approach for the quantitative sensing of nitroaromatics, particularly TNT, using morphologically different self-assemblies of a carbazole bridged fluorene (CBF) derivative is described. Picomolar level detection of TNT was possible in water by the CBF nanoparticles and nanogram level TNT sensing in vapour phase could be achieved with the CBF supramolecular rods.

Introduction

Detection of nitroaromatics, particularly trinitrotoluene (TNT) has been of interest due to its importance in security and environmental safety control.[1] Fluorescence quenching based technique is preferred in molecular sensing because of its high sensitivity, and ease of execution.[2] Therefore, a number of self-assembled fluorescent materials constructed from organic molecules having efficient excited state energy migration and strong interaction with a target analyte have been tested for chemosensing application.[3] In this context, the most widely used organic materials for sensing are either of zero-dimensional (0D) particles[4] or one-dimensional (1D) nanostructures (fibres, rods, etc.)[5]. Trogler and co-workers reported an oligo(tetraphenyl)silole based nanoparticles suspended in water with aggregation induced emission properties for the sensing of TNT at ppb level in aqueous environment.[4a] Previously, we have reported self-assembled fibrils of a molecular gelator with good solid-state fluorescence quantum yield for sensing TNT vapours with high sensitivity.[5c] Upon deposition to a substrate, these nanostructures could entrap nitroaromatic analyte vapours during exposure. An efficient exciton migration (via intermolecular π-electronic coupling) to the entrapped analyte facilitates fast signalling of the sensing event.[3a,5b,c] In many cases, interaction of a target analyte with self-assembled nanostructures is strongly influenced by the morphological features of the assemblies.[6] Therefore, a deeper understanding of the morphology assisted sensing of analytes with self-assembled molecular architecture is of great relevance. Moreover, quantitative detection of the adsorbed analyte vapour by a sensor is required in many cases for which quartz-crystal microbalance (QCM) is a suitable method.[7] Herein, a combined fluorescence and QCM approach is described for the sensing as well as the estimation of TNT in vapour phase. We primarily focus on the role of the morphological features of the self-assembled nanostructures on sensing and quantification of adsorbed TNT vapours.

Experimental Details

Synthesis

Unless otherwise stated, all materials and reagents were purchased from commercial suppliers. The solvents and reagents were purified and dried by standard methods prior to use. 2,4-Dinitrotoluene (DNT) was purchased from TCI and recrystallized from ethanol. TNT was synthesised as per the reported procedure and recrystallized from ethanol.[6b,8] Compounds **1**-**7** (Scheme 1) were prepared by following the previously reported procedures.[9]

Synthesis of **CBF** – Compound **8** (1.2 g, 0.78 mmol) was dissolved in anhydrous CH_2Cl_2 (20 mL) by stirring at room temperature under argon atmosphere. *N,N'*-diisopropyl-

ethylamine (0.34 mL, 1.95 mmol) and acetic acid (117 mg, 1.95 mmol, 2.5 equiv.) were added to the above solution and stirred for 30 minutes. The reaction mixture was cooled to 0 ℃ using an ice-salt bath and stirring was continued for another 10 minutes. HATU (741 mg, 1.95 mmol) was added to the reaction mixture and the temperature was allowed to increase gradually followed by stirring at room temperature for 6 h. Then the reaction mixture was poured into water and extracted with CH_2Cl_2. The combined organic layer was dried over anhydrous Na_2SO_4 and evaporated to dryness under reduced pressure. The resulting crude product was purified by silica gel (100-200 mesh) column chromatography using, CH_2Cl_2/hexane (8/2) as an eluent afforded pure **CBF** as an off-white solid in 75% yield. M.p.: 134± 2 °C. FT-IR (KBr): ν_{max} = 1125, 1259, 1321, 1371, 1411,1456, 1541, 1591, 1657, 2849, 2924, 3305 cm^{-1}; ^1H NMR (500 MHz, $CDCl_3$, TMS, 25 °C): 0.84–0.88 (t, 15H; -CH_3), 1.08–1.28 (m, 100H; -CH_2-), 1.59–1.62 (t, 8H; -CH_2-), 2.23 (s, 6H; -NH-CH_3), 4.44–4.75 (t, 2H; -N-CH_2), 7.27–7.29 (d, 2H; Ar-*H*), 7.49–7.51 (d, 2H; Ar-*H*), 7.55–7.57 (d, 2H; Ar-*H*), 7.60 (s, 2H; Ar-*H*), 7.66-7.77 (m, 10H; Ar-*H*), 8.18-8.20 (d, 2H; Ar-*H*) ppm; ^{13}C NMR (125 MHz, $CDCl_3$, 25 °C): δ = 14.12, 22.68, 23.91, 24.83, 27.47, 29.12, 29.34, 29.47, 29.61, 29.65, 29.70, 30.13, 31.91, 40.47, 43.11, 55.38, 76.82, 77.03, 77.24, 107.19, 114.41, 118.48, 118.80, 119.56, 120.09, 120.55, 121.89, 121.95, 126.45, 137.16, 139.62, 139.85, 140.72, 141.65, 151.38, 152.22, 168.05 ppm; MALDI-TOF-MS (matrix: α-cyano-4-hydroxycinnamic acid): m/z calcd. for $C_{102}H_{151}N_3O_2$ $[M]^+$: 1451.18; found: 1451.77.

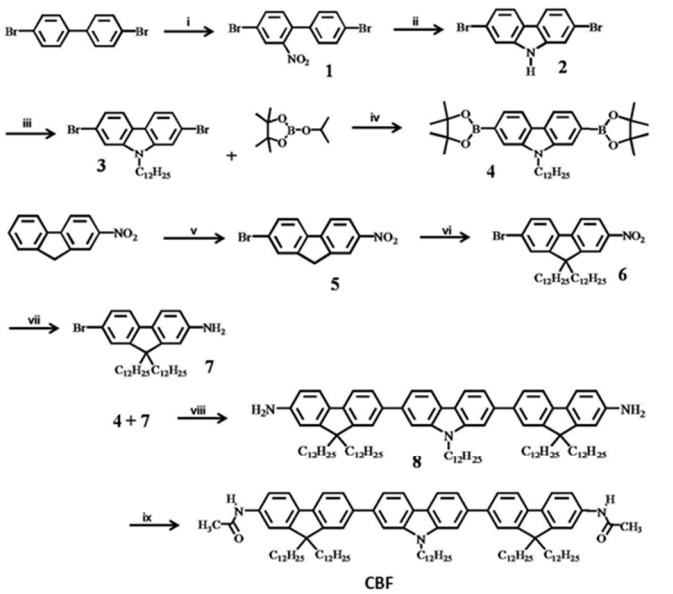

Scheme 1. Multi-step procedure for the preparation of **CBF**. Reagents and conditions: (i) HNO_3, 100 °C, 30 min, 92%; (ii) $P(OC_2H_5)_3$, reflux, 18 h, 55%; (iii) $C_{12}H_{25}Br$, NaH, DMF, rt, 18 h, 95%; (iv) *n*-BuLi, THF, -78 °C and rt, 12 h, 64%; (v) Br_2, CH_2Cl_2, rt, 12 h, 67%; (vi) DMSO, KOH, KI, $C_{12}H_{25}Br$, rt, 12 h, 58%; (vii) $SnCl_2$, EtOH/EtOAc (1:1), reflux, 12 h, 90%; (viii) $Pd(PPh_3)_4$, K_2CO_3, THF/water (2:1), 90 °C, 48 h, 70%; (ix) CH_3COOH, N,N'-diisopropylethylamine, O-(7-azabenzotriazol-1-yl)-N,N,N',N'-tetramethyl uronium hexafluorophosphate (HATU), CH_2Cl_2, 0 °C- rt, 12 h, 75%.

Materials and methods

SPECTRAL MEASUREMENTS: The absorption spectra were recorded on a Shimadzu UV-Vis recording spectrophotometer UV-2100. Film state measurements were performed using $BaSO_4$ as standard. The emission spectra were recorded on a SPEX-Flourolog F112X spectrofluorimeter with a 1 cm cuvette. Film state samples were performed using a front face sample holder.

FIELD-EMISSION SCANNING ELECTRON MICROSCOPY (FE-SEM): FE-SEM measurements were carried out using a Hitachi S-4800 at an accelerating voltage of 15 kV after sputtering with platinum. Samples for the SEM were prepared on a silicon-wafer substrate that was pasted above an aluminium stub by using a conductive carbon tape. The samples were prepared by spin coating (3000 rpm for 60 s) at required concentrations and kept in a closed chamber under vacuum for overnight.

ATOMIC FORCE MICROSCOPY (AFM): AFM images were recorded under ambient conditions using a NTEGRA (NT-MDT) operating with a tapping mode regime. Micro-fabricated TiN cantilever tips (NSG10) with a resonance frequency of 299 kHz and a spring constant of 20-80 Nm^{-1} were used. AFM section analysis was done offline. Samples for the imaging were prepared by drop casting the solution on freshly cleaved mica surface at the required concentrations at ambient conditions.

Confocal Laser Scanning Microscopy (CLSM): CLSM images were recorded on a Leica-DMIR2 optical microscope using UV light (380 nm) as the excitation source and the emission was collected between 450 nm to 550 nm with 10x magnification. Samples were prepared by drop casting the solution on a glass slide followed by slow evaporation.

DYNAMIC LIGHT SCATTERING (DLS): Particle size analysis was carried out using a Photal Otsuka Electronics DLS-6000AL instrument. Organic nanoparticles in aqueous medium were prepared as follows. 5 mL Milli-Q water was taken in a 15 mL glass vial and stirred at 1500 rpm using a magnetic bead and stirrer. **CBF** dissolved in THF (0.5×10^{-3} M) were taken in a syringe (50–200 mL) and injected into the stirring water. Stirring was continued for another 1 min to yield a stable nanoparticle suspension in water.

QUARTZ CRYSTAL MICROBALANCE (QCM): The QCM technique was used for detection of mass change during the adsorption of analytes vapour. The resonance frequency was 9 MHz (AT-cut). The frequency of the QCM electrode was measured for adsorption step. The frequency was recorded when it became stable. The QCM frequency in air was stable within ±2 Hz during 1h. The time-dependence of frequency change (Δf) were plotted during the alternate exposure. All experiments were carried out in an air-conditioned room at 25 °C.

QCM is sensitive to mass change, when the surface of a quartz crystal electrode is coated with a coating material. The change in mass m (gcm^{-2}) of sample layer deposited onto QCM electrode can be measured by the oscillating frequency of the quartz electrode. The frequency change (Δf) corresponds to the

sample amount loaded on the QCM electrode, which can be calculated from Sauerbrey equation:[7a]

$$\Delta f = -\left(2f_0^2 \middle| \sqrt{\rho_Q \, \mu_Q}\right) m$$

where f_o (Hz) is the natural frequency of the quartz crystal, ρ_Q is the quartz density (2.649 gcm^{-3}), and μ_Q is the shear modulus (2.947 × 1011 gcm^{-1}s^{-2}).

Preparation of CBF self-assemblies: A hot solution of **CBF** in MCH (0.1 mM) was cooled to 0 ℃ by dipping in an ice-bath for 10 min. to yield rods of varying size. The **CBF** nanoparticles were prepared by injecting 50 µL of 1 mM THF solution to a 5 mL stirring water (at 1500 rpm) in a 15 mL vial. The stirring was continued for 5 min more. Rods and particles formations were confirmed by FE-SEM and AFM analyses.

Detection of TNT vapours by emission quenching: The **CBF** rods or particles were prepared as described above, drop cast over glass plates and dried under vacuum. The film was placed in a chamber containing saturated TNT vapour. Emission was collected by using a front face technique using a film sample holder.

Detection of TNT in potable water by emission quenching: A stock solution (5 × 10^{-4} M) was prepared by dissolving TNT in potable water by overnight stirring at room temperature (0.114 mg/mL). This solution was diluted to different concentrations and used as the test samples (1 × 10^{-15} M – 1 × 10^{-3} M). The **CBF** rods or nanoparticles solutions were added to the TNT solutions and the fluorescence intensities were measured. The minimum detection level of TNT was qualitatively judged by fluorescence quenching (< 5%) on the solution.

Results and discussion

Carbazole based building blocks are electron rich and highly fluorescent which are sensitive to nitroaromatics.[10] On the other hand, fluorene based systems are known to form 0D and 1D aggregates under different experimental conditions.[11,12] In order to combine these two properties in a single system, we designed and synthesized the amide end functionalised carbazole-fluorene molecular hybrid (**CBF**) (Scheme 1) and prepared different supramolecular architectures for the detection of TNT. **CBF** was synthesized according to Scheme 1 and characterised by FT-IR, ^{1}H and ^{13}C NMR, and MALDI-TOF spectroscopic methods. The electronic spectra of **CBF** at a conc. of 5 × 10^{-5} M in tetrahydrofuran (THF) exhibited an absorption maximum at 363 nm and emission peaks at 408 and 427 nm (Fig. S1, ESI†). In methylcyclohexane (MCH, 5 × 10^{-5} M), **CBF** showed a blue shift for absorption (5 nm) and emission maximum (4 nm) with a reduction in intensity. It is found that **CBF** self-assembles to form rods in MCH and nanoparticles from water. Upon excitation with UV light (λ_{ex} = 370 nm), nanoparticles showed a weak blue fluorescence (Fig. S2, ESI†).

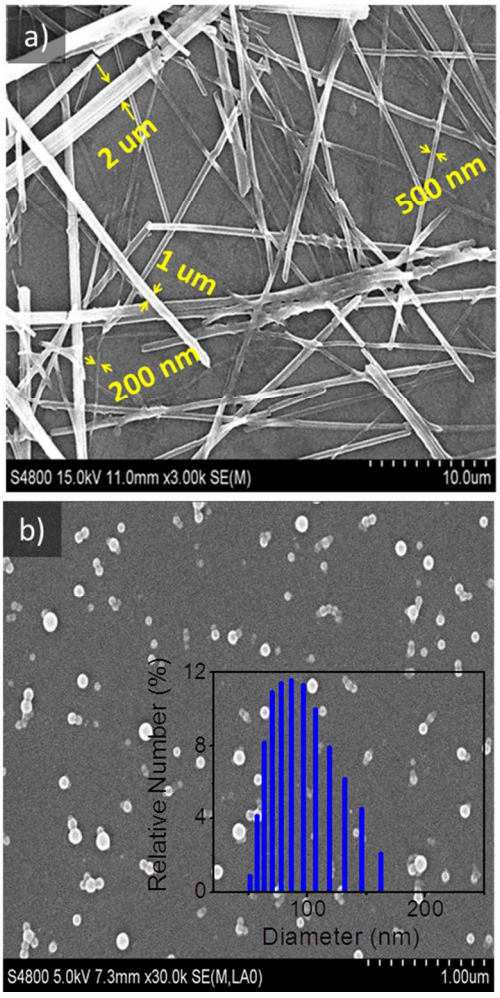

Fig. 2 FE-SEM images of (a) **CBF** rods from MCH solution (5 × 10^{-5} M) and (b) **CBF** nanoparticles suspension in water (1 × 10^{-5} M), inset shows the particle size distribution of **CBF** nanoparticles by DLS analysis.

CBF is soluble in most of the common organic solvents except in MCH at a concentration of 1 × 10^{-4} M. Interestingly we observed a weak gelation of **CBF** in MCH (2 mM) upon heating followed by cooling in an ice-bath. Supramolecular rod formation was observed within the concentration ranges from 0.1 - 1 mM of **CBF** in MCH. Upon excitation with UV light (λ_{ex} = 370 nm), rods showed a bright blue fluorescence. Self-assembled rod and nanoparticle formation was further confirmed with atomic force microscopy (AFM), and field-emission scanning electron microscopy (FE-SEM). The FE-SEM analysis of **CBF** self-assembly in MCH displayed rods (Fig. 2a) having width of 0.2 - 2 µm and length of several micrometers. This morphology was also verified by AFM analyses (Fig. S3, ESI†). The microscopic images of nanoparticles revealed an average particle size of 100 nm (Fig. 2b and Fig. S3, ESI†) which was supported by dynamic light scattering (DLS) experiment (Fig. 2b inset).

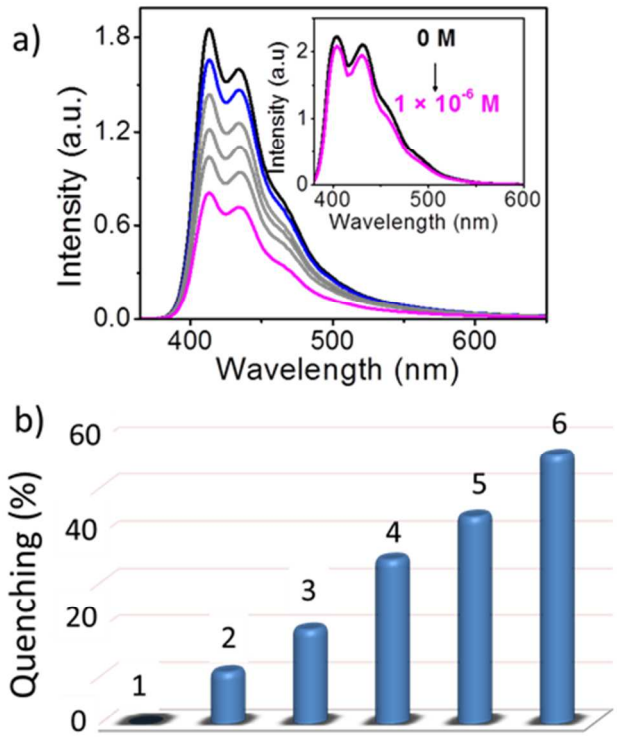

Fig. 3 (a) Fluorescence quenching of **CBF** nanoparticle suspension in water by the addition of 1×10^{-12} (—) - 1×10^{-6} M (—) TNT solution in water; inset shows the fluorescence quenching of **CBF** in THF (1×10^{-5} M) upon addition of 1×10^{-6} M TNT solution (—). (b) Plot of fluorescence quenching vs concentration, 1 (**CBF** alone), 2 (1×10^{-12} M), 3 (1×10^{-10} M), 4 (1×10^{-8} M), 5 (1×10^{-7} M), 6 (1×10^{-6} M) of added TNT solutions. (λ_{ex} = 370 nm, l = 1 cm).

Since **CBF** formed fluorescent nanoparticles in water, we first checked whether this material can be used for testing the contamination of water by nitro aromatics, particularly TNT. The fluorescence intensity variation of **CBF** nanoparticles in water in presence of TNT is shown in Fig. 3a. Upon addition of 1×10^{-12} - 1×10^{-6} M TNT solution in water, a gradual quenching of the emission occurred, reaching a maximum quenching of 50% at 1×10^{-6} M TNT (Fig. 3a). The lowest detection limit of TNT was in picomolar level (10^{-12} M). Addition of similar concentrations of TNT to a THF solution of **CBF** showed <5% quenching of fluorescence (Fig. 3a inset) revealing the importance of the **CBF** nanoparticles in TNT sensing. A plot of the percentage fluorescence quenching with different concentrations of TNT is shown in Fig. 3b. The selectivity coefficient of nanoparticles for TNT over RDX was ~10 indicating the strong affinity of **CBF** to nitroaromatics when compared to non-aromatic nitro compounds. Similarly, high selectivity coefficient was observed (~10) for TNT versus aromatics compounds with strong acceptors such as cyano, chloro, etc., confirming the selective interaction of **CBF** nanoparticles with nitroaromatics in water.

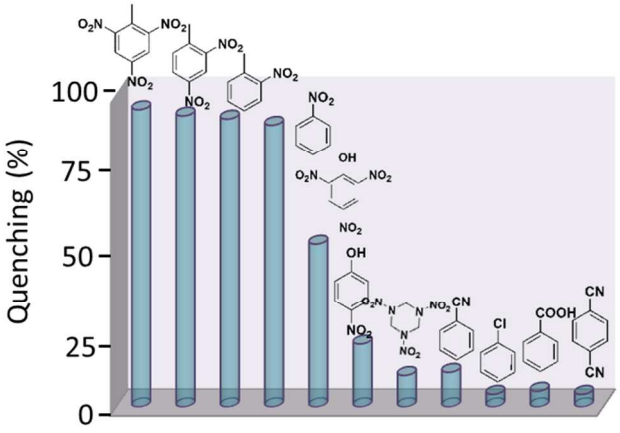

Fig. 4 a) Plot of fluorescence quenching percentage (monitored at 405 nm) of **CBF** nanoparticles (1×10^{-5} M) upon addition of 1 equiv. of different analytes (λ_{ex} = 370 nm).

To further calculate the limit of detection and limit of quantification, we followed a method reported by Hakonen and co-workers.[13] A picomolar calibration was performed for **CBF** nanoparticle in water as shown in Fig. 5. The zero level standard deviation (SD_{zero}) was calculated as 0.15 and slope from zero to the picomolar conc. of TNT was calculated as 1.9×10^{12}. From the slope between 0 and 1 pM concentration of TNT and the standard deviation of the zero level (i.e., standard approximation 3 × SD_{zero}/slope) the limit of detection was calculated as 0.23 pm and limit of quantification was calculated as 0.78 pm (10 × SD_{zero}/slope). In order to check the possible interaction with other nitroaromatics we have monitored the fluorescence quenching of **CBF** nanoparticles with 2,4-dinitrotoluene (DNT) in water (Fig. S4, ESI†). As observed with TNT, a significant quenching of the fluorescence was observed with DNT, indicating that **CBF** nanoparticles are not selective to a particular nitroaromatic compound. Further, selectivity towards nitroaromatics was demonstrated by testing other common analytes with **CBF** nanoparticles in water (1×10^{-5} M). Negligible fluorescence changes were observed for non-nitroaromatics, whereas significant quenching was observed for other nitroaromatics (Fig. 4).

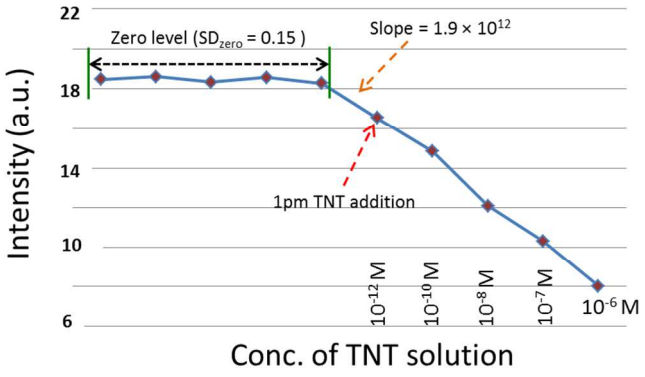

Fig. 5 Fluorescence calibration curve for **CBF** nanoparticles before (blank) and after addition of TNT (from picomolar range).

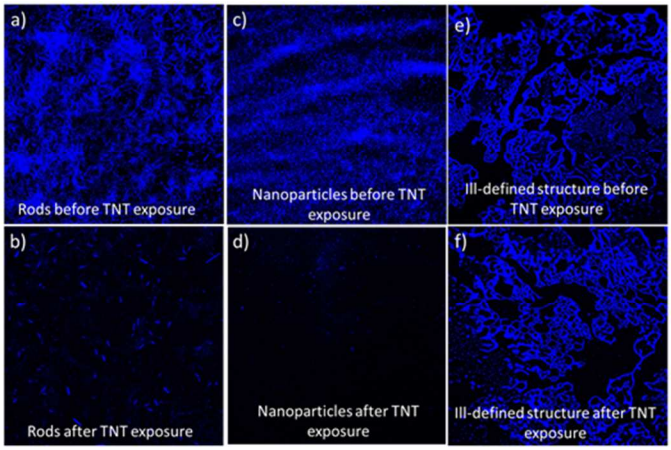

Fig. 6 CLSM images of film from MCH (a,b), water (c,d) and THF (e,f), before (a,c,e) and after (b,d,f) exposure to TNT vapours for 10 min.

Vapour phase sensing of TNT by the **CBF** assemblies were monitored with a confocal laser scanning microscopic (CLSM). Exposure of TNT vapour for a period of 10 min showed significant decrease in the fluorescence intensity of the rods whereas only negligible changes were observed for the ill-defined molecular aggregates obtained from THF solution (Fig. S6, ESI†). The CLSM images of the different **CBF** assemblies before and after exposure with TNT vapours revealed the supremacy of the defined structures over the ill-defined molecular aggregates on fluorescence response. Selectivity coefficient was high for nitroaromatics (5-10) when compared to other analytes indicating the strong affinity of **CBF** rods (donor) to the nitroaromatics (acceptor).

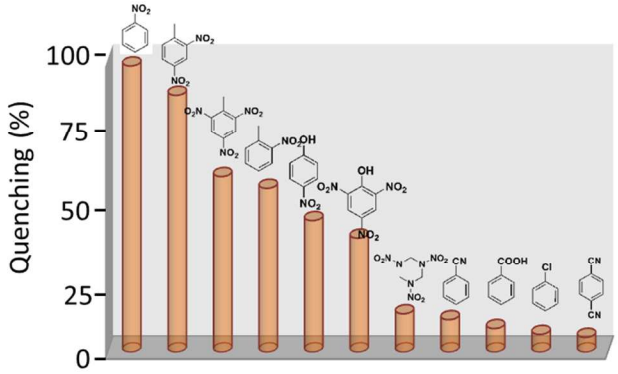

Fig. 7 Plot of % quenching of fluorescence monitored at 405 nm of CBF rods upon exposure to different analytes for a period 10 m (λ_{ex} = 370 nm).

Similar to **CBF** nanoparticles, **CBF** rods also showed selectivity towards nitro aromatic compounds (Fig. 7). In the film state, within 30 s, 24% fluorescence quenching was observed for rods and 15% quenching for nanoparticles when exposed to TNT vapours (Fig. 8a). Within 5 min, nanoparticles overtake the fluorescence quenching efficiency when compared to that of the **CBF** rods. About 45 % and 60% quenching were observed within 10 min for rods and nanoparticles respectively (Fig. 8a). However, the ill-defined molecular aggregates from THF showed no quenching for the initial 30 s, however, a 24% quenching was observed after 10 min (Fig. 8a). The fluorescence response observed with DNT vapours was better when compared to that of TNT, which may be due to the high vapour pressure of the former (Fig. S6, ESI†).

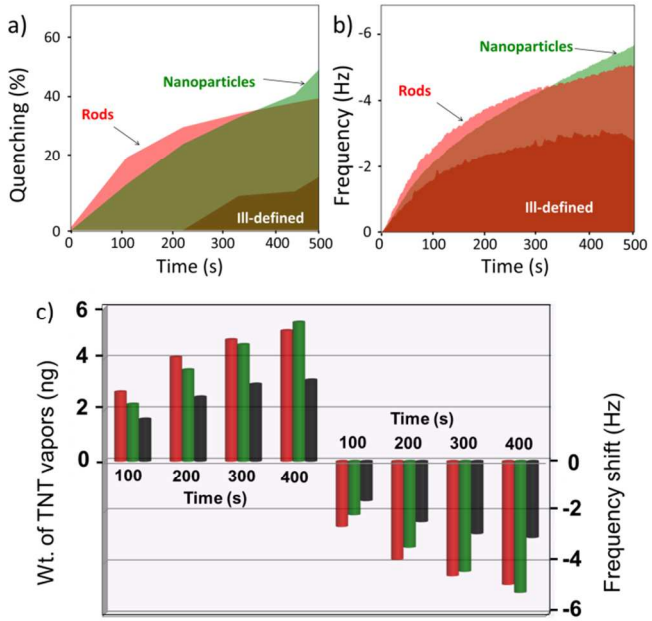

Fig. 8 (a) A plot of fluorescence quenching percentage vs time (b) frequency shift of quartz crystal vs time and (c) weight of TNT vapours adsorbed (upward) and corresponding frequency shift (downward) of a QCM crystal coated with CBF rods (—), nanoparticles (—) and ill-defined molecular aggregates (—) upon exposing to TNT vapour.

The marginally better fluorescence quenching by the self-assembled rods over the nanoparticles at the initial stage of exposure to TNT vapours may be due to the better excited state energy migration in 1D rods which amplifies the sensing process even with small amount of the analyte. Upon continued exposure to TNT vapours, the nanoparticles showed better quenching efficiency probably due to the better diffusion of TNT vapour due to the large surface area of the nanoparticles. In order to get more insights into the amount of adsorbed TNT vapour on **CBF** nanostructures, we performed QCM experiments. As shown in Fig. 8a the frequency of quartz crystal decreases with time, which is an indication of adsorption of TNT vapours. After 100 s, the self-assembled rods showed 2.58 ng of TNT adsorption registering a 38% fluorescence quenching and 2.12 ng of TNT adsorption by nanoparticles exhibiting a 35% fluorescence quenching. Interestingly, the ill-defined **CBF** aggregates could adsorb only 1.59 ng of TNT with a 7 % fluorescence quenching (for details see Table S1 ESI†). After 200 s the ill-defined structure showed 2.39 ng of TNT intake (Fig. 8b), however, the quenching efficiency was only about 10% (Fig. 6a). The poor fluorescence quenching of the ill-defined structure when compared to the rods (40%, 3.86 ng of TNT) and nanoparticles (41%, 3.4 ng of TNT), indicates that even a subtle variation in the morphological features of the self-assembly can make significant change in the fluorescence quenching process. After 500 s, the amount of TNT adsorbed

on nanoparticles was more with enhanced fluorescence quenching (64%) when compared to rods (45%). It is well documented in literature that the excited state energy migration assisted electron transfer (amplified quenching[2a]) in self-assembled materials enhances the sensing efficiency.[3,5c] As described earlier, carbazole based assemblies are known as good donor material and the quenching of **CBF** fluorescence upon vapour exposure must be due to an electron transfer from **CBF** to TNT.

Conclusions

In conclusion, we have demonstrated the TNT sensing ability of a fluorescent molecular hybrid **CBF** which is self-assembled into different morphological forms. The aqueous suspension of **CBF** nanoparticles has been found useful for the detection of TNT in water with a picomolar level sensitivity. **CBF** supramolecular rods have been used to detect TNT vapours in nanogram level. When compared to the ill-defined molecular aggregates, the nanoparticles and rods showed amplified fluorescence quenching towards TNT vapours. It is important to note that **CBF** rods are better suited for the detection of TNT due to the relatively fast response at lower time scale with small amount of TNT vapours. A quantitative detection of the adsorbed TNT by QCM technique on these nanostructures reveals the importance of the morphological features of the self-assembled supramolecular structures for the sensing of various analytes.

Acknowledgements

K.K.K., M.T. and A.A. thank the Department of Science and Technology, Government of India and the Japan Society for the Promotion of Science, Japan for financial support under a bilateral exchange programme. We thank Dept. Atomic Energy, Government of India for a DAE-SRC Outstanding Researcher Award to A.A. K.K.K. and A.S. are grateful to the CSIR for fellowship. We acknowledge Dr. K. Ariga and Dr. Q. Ji (NIMS) for the QCM analysis, Dr. S. Ogi (NIMS) for FE-SEM analysis.

Notes and references

[a]*Photosciences and Photonics Group, Chemical Sciences and Technology Division, CSIR-National Institute for Interdisciplinary Science and Technology (CSIR-NIIST), Trivandrum 695 019, India.*
[b]*Organic Materials Group, Polymer Materials Unit, National Institute for Materials Science (NIMS), 1-2-1 Sengen, Tsukuba, 305-0047, Japan.*
E-mail: TAKEUCHI.Masayuki@nims.go.jp

† Electronic Supplementary Information (ESI) available: [Absorption, emission profiles, fluorescence quenching profiles, and AFM images]. See DOI: 10.1039/b000000x/

1. (*a*) A. Rose, Z. Zhu, C. F. Madigan, T. M. Swager and V. Bulovic, *Nature*, 2005, **434**, 876-879; (*b*) Y. Salinas, R. Martinez-Manez, M. D. Marcos, F. Sancenon, A. M. Costero, M. Parra and S. Gil, *Chem. Soc. Rev.*, 2012, **41**, 1261-1296.
2. (*a*) S. W. Thomas, G. D. Joly and T. M. Swager, *Chem. Rev.*, 2007, **107**, 1339-1386; (*b*) M. E. Germain and M. J. Knapp, *Chem. Soc. Rev.*, 2009, **38**, 2543-2555; (*c*) B. Gole, S. Shanmugaraju, A. K. Bar and P. S. Mukherjee, *Chem. Commun.,* 2011, **47**, 10046-10048; (*d*) N. Venkatramaiah, S. Kumar and S. Patil, *Chem.–Eur. J.*, 2012, **18**, 14745-14751; (*e*) S. S. Nagarkar, B. Joarder, A. K. Chaudhari, S. Mukherjee and S. K. Ghosh, *Angew. Chem., Int. Ed.*, 2013, **52**, 2881-2885.
3. (*a*) L. Zang, Y. K. Che and J. S. Moore, *Acc. Chem. Res.*, 2008, **41**, 1596-1608; (*b*) Y. K. Che and L. Zang, *Chem. Commun.*, 2009, 5106-5108; (*c*) Y. K. Che, D. E. Gross, H. L. Huang, D. J. Yang, X. M. Yang, E. Discekici, Z. Xue, H. J. Zhao, J. S. Moore and L. Zang, *J. Am. Chem. Soc.*, 2012, **134**, 4978-4982; (*d*) X. Huang, X. Gu, G. Zhang and D. Zhang, *Chem. Commun.*, 2012, 48, 12195-12197; (*e*) V. Bhalla, S. Pramanik and M. Kumar, *Chem. Commun*., 2013, **49**, 895-897; (*f*) N. Dey, S. K. Samanta and S. Bhattacharya, *ACS Appl. Mater. Interfaces*, 2013, **5**, 8394-8400.
4. (*a*) S. J. Toal, D. Magde and W. C. Trogler, *Chem. Commun.*, 2005, 5465-5467; (*b*) S. J. Toal, K. A. Jones, D. Magde and W. C. Trogler, *J. Am. Chem. Soc.*, 2005, **127**, 11661-11665.
5. (*a*) T. Naddo, Y. K. Che, W. Zhang, K. Balakrishnan, X. M. Yang, M. Yen, J. C. Zhao, J. S. Moore and L. Zang, *J. Am. Chem. Soc.*, 2007, **129**, 6978-6979; (*b*) Y. K. Che, X. M. Yang, G. L. Liu, C. Yu, H. W. Ji, J. M. Zuo, J. C. Zhao and L. Zang, *J. Am. Chem. Soc.*, 2010, **132**, 5743-5750. (*c*) K. K. Kartha, S. S. Babu, S. Srinivasan and A. Ajayaghosh, *J. Am. Chem. Soc.*, 2012, **134**, 4834-4841.
6. (*a*) L. Wang, Y. Zhou, J. Yan, J. Wang, J. Pei, and Y. Cao, *Langmuir*, 2009, **25**, 1306-1310; (*b*) C. Vijayakumar, G. Tobin, W. Schmitt, M. J. Kim and M. Takeuchi, *Chem. Commun.*, 2010, **46**, 874-876.
7. (*a*) G. Sauerbrey, *Z. Phys.*, 1959, **155**, 206-222; (*b*) W. H. K. Jr., *Anal. chem.*, 1964, **36**, 1735-1739; (*c*) Q. M. Ji, I. Honma, S. M. Paek, M. Akada, J. P. Hill, A. Vinu and K. Ariga, *Angew. Chem., Int. Ed.*, 2010, **49**, 9737-9739; (*d*) J. R. Cox, P. Muller and T. M. Swager, *J. Am. Chem. Soc.*, 2011, **133**, 12910-12913; (*e*) N. Bachar, L. Mintz, Y. Zilberman, R. Ionescu, X. Feng, K. Müllen and H. Haick, *ACS Appl. Mater. Interfaces* 2012, **4**, 4960-4965; (*f*) Bachar, L. Liberman, F. Muallem, X. Feng, K. Müllen and H. Haick, *ACS Appl Mater Interfaces* 2013, **5**, 11641-11653.
8. R. C. Dorey and W. R. Carper, *J. Chem. Eng. Data*, 1884, **29**, 93.
9. (*a*) F. Dierschke, A. C. Grimsdale and K. Müllen, *Synthesis*, 2003, 2470-2472. (*b*) M. Sonntag and P. Strohriegl, *Chem. Mater.*, 2004, **16**, 4736-4742. (*c*) R. Abbel, C. Grenier, M. J. Pouderoijen, J. W. Stouwdam, P. E. L. G. Leclere, R. P. Sijbesma, E. W. Meijer and A. P. H. J. Schenning, *J. Am. Chem. Soc.*, 2009, **131**, 833-843. (*d*) B. Balan, C. Vijayakumar, S. Ogi and M. Takeuchi, *J. Mater. Chem.*, 2012, **22**, 11224-11234.
10. (*a*) C. Y. Zhang, Y. K. Che, X. M. Yang, B. R. Bunes and L. Zang, *Chem. Commun.*, 2010, **46**, 5560-5562; (*b*) H. R. Nie, G. N. Sun, M. Zhang, M. Baumgarten and K. Müllen, *J. Mater. Chem.*, 2012, **22**, 2129-2132; (*c*) G. Q. Tang, S. S. Y. Chen, P. E. Shaw, K. Hegedus, X. Wang, P. L. Burn and P. Meredith, *Polym. Chem.*, 2011, **2**, 2360-2368.
11. R. Abbel, R. van der Weegen, W. Pisula, M. Surin, P. Leclere, R. Lazzaroni, E. W. Meijer and A. P. H. J. Schenning, *Chem.–Eur. J.*, 2009, **15**, 9737-9746.
12. (*a*) R. Abbel, R. van der Weegen, E. W. Meijer and A. P. H. J. Schenning, *Chem. Commun.*, 2009, 1697-1699. (*b*) Kaeser and A. P. H. J. Schenning, *Adv. Mater.* 2010, **22**, 2985-2997; (*c*) Vijayakumar, K. Sugiyasu and M. Takeuchi, *Chem. Sci.*, 2011, **2**, 291-294; (*d*) A.

L. Stevens, A. Kaeser, A. P. H. J. Schenning and L. M. Herz, *ACS Nano*, 2012, **6**, 4777-4787; (*e*) B. Balan, C. Vijayakumar, S. Ogi and M. Takeuchi, *J. Mater. Chem.*, 2012, **22**, 11224-11234.

13. (*a*) A. Hakonen, *Anal. Chem.*, 2009, **81**, 4555-4559; (*b*) A. Hakonen and N. Stromberg, *Analyst*, **137**, 315-321; (*c*) A. Hakonen, J. E. Beves and N. Stromberg, *Analyst*, 2014, **139**, 3524–3527.

Table of Contents

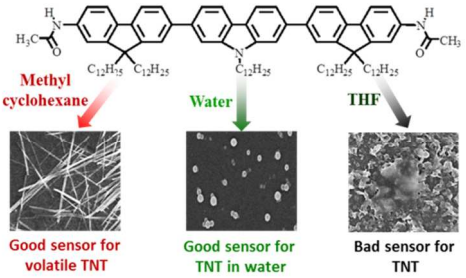

Self-assembled fluorescent rods and nanoparticles prepared from a carbazole-fluorene molecular hybrid have been used for the sensing of TNT. A combined fluorescence quenching and quartz crystal microbalance approach has been used for the quantitative sensing of TNT by the self-assembled rods.